Hydrol. Earth Syst. Sci. Discuss., 9, 405–440, 2012
www.hydrol-earth-syst-sci-discuss.net/9/405/2012/
doi:10.5194/hessd-9-405-2012

Hydrology and Earth System Sciences Discussions

Development and validation of a global dynamical wetlands extent scheme

T. Stacke and S. Hagemann

Max-Planck-Institut für Meteorologie, Germany

Received: 13 December 2011 – Accepted: 16 December 2011 – Published: 10 January 2012

Correspondence to: T. Stacke (tobias.stacke@zmaw.de)

Published by Copernicus Publications on behalf of the European Geosciences Union.

Abstract

In this study we present the development of the dynamical wetland extent scheme (DWES) and its validation against present day wetland observations. The DWES is a simple, global scale hydrological scheme that solves the water balance of wetlands and estimates their extent dynamically. The extent depends on the balance of water flows in the wetlands and the slope distribution within the grid cells. In contrast to most models, the DWES is not directly calibrated against wetland extent observations. Instead, wetland affected river discharge data are used to optimize global parameters of the model. The DWES is not a complete hydrological model by itself but implemented into the Max Planck Institute – Hydrology Model (MPI-HM). However, it can be transferred into other models as well.

For present climate, the model validation reveals a good agreement between the occurrence of simulated and observed wetlands on the global scale. The best result is achieved for the northern hemisphere where not only the wetland distribution pattern but also their extent is simulated reasonably well by the DWES. However, the wetland fraction in the tropical parts of South America and Central Africa is strongly overestimated. The simulated extent dynamics correlate well with monthly inundation variations obtained from satellite for most locations. Also, the simulated river discharge is affected by wetlands resulting in a delay and mitigation of peak flows. Compared to simulations without wetlands, we find locally increased evaporation and decreased river flow into the oceans due to the implemented wetland processes.

In summary, the validation analysis demonstrates the DWES' ability to simulate the global distribution of wetlands and their seasonal variations. Thus, the dynamical wetland extent scheme can provide hydrological boundary conditions for wetland related studies. In future applications, the DWES should be implemented into an earth system model to study feedbacks between wetlands and climate.

HESSD
9, 405–440, 2012

1 Introduction

In recent studies wetlands are suspected to play an important role during periods of climate change (e.g. Friedlingstein et al., 2011; Gedney et al., 2004; Levin et al., 2000). However, the representation of the wetland's spatial extent and seasonality is a weak point in today's climate models and needs to be improved by a better simulation of their hydrological cycle (O'Connor et al., 2010; Ringeval et al., 2010).

The water table depth in wetlands is an important factor for the wetland's biogeochemistry leading to carbon sequestration or decomposition (e.g. O'Connor et al., 2010, and references therein). While most of them are seen as net carbon sinks for today's climate conditions (Bohn et al., 2007; Gorham, 1991; Friborg et al., 2003), a number of studies concluded that some wetlands might turn into carbon sources in a warmer climate (St-Hilaire et al., 2010; Gorham, 1991).

Furthermore, the wetland hydrology in itself is an important key factor in the climate system. On the one hand, surface water has to be considered in climate models because of its feedbacks to the atmosphere (Coe and Bonan, 1997). The effect of open water surfaces on the energy and water balance was investigated by several studies, e.g. Bonan (1995) and Mishra et al. (2010), who reported a significant impact of wetlands on the local climate. On the other hand, wetlands interact in several ways with the hydrological cycle of their surrounding area (e.g. Bullock and Acreman, 2003). These processes are of high interest for impact studies that investigate how climate change might effect the water storage capacities in a region or the characteristics of river flooding.

While a number of models exist which do simulate wetland extent dynamics, only few of them are designed for the application on global scale. Among these are simple schemes focusing only on soil moisture and slope (Kaplan, 2002) as well as more sophisticated enhancements of the TOPMODEL approach (e.g. Gedney et al., 2004; Kleinen et al., 2011). While these models usually lack an explicit surface water storage, this feature is included in a dynamic inundation model by Decharme et al. (2008,

HESSD
9, 405–440, 2012

2011). Very often model approaches are strongly depending on detailed soil properties information (e.g. Bowling and Lettenmaier, 2010; Yu et al., 2006) or are calibrated for specific catchments (e.g. Bohn et al., 2007). Thus, the main objective of this study is the development of a globally valid hydrological scheme that represents a realistic water cycle for wetlands and computes their extent and distribution dynamically. The explicit requirements for the dynamical wetland extent scheme (DWES) are to use a more general approach for the wetland dynamics calculation which is independent of fine scale boundary data such as soil conductivity or porosity. Additionally, the model should not be calibrated against today's wetland extent observations and, hence, should be applicable under different climate conditions. Consequently, the DWES can also be used for paleoclimate simulations which lack detailed land surface boundary data.

During the development and validation of the model, we have been using four global wetland observation maps to evaluate the simulation performance of the DWES. These are a satellite derived inundation dataset (SIND) (Prigent et al., 2001, 2007), the Global Lake and Wetland Database (GLWD) (Lehner and Döll, 2004), the Land Surface Parameter set 2 (LSP2) (Hagemann et al., 1999; Hagemann, 2002) and a wetland ecosystem map (MATT) (Matthews and Fung, 1987). It has to be noted that the data sets differ in their definition of wetlands as well as in the methodology which has been used to derive the wetland extent. Furthermore, the are not completely consistent with the wetland definition used in the DWES. For this reason, we do not use the wetland observations directly. Instead we aim to increase the robustness of observations and the comparability to our wetland simulation by calculating an esemble mean of observations which is then applied in our analyzes. While the SIND displays monthly values of inundation extent, the remaining datasets show the maximum wetland extent throughout the year. Thus, we computed the same quantity for the SIND before deriving the ensemble mean of all observations.

The first part of this paper is concerned with the development of the DWES. Here, we give detailed information about its basic approach and the parameter optimization. In the second part the model is validated against global wetland observations focusing

HESSD
9, 405–440, 2012

more on simulated large scale wetlands instead of grid cell results. In the third part we elaborate on possible feedbacks which can be simulated by our model and on its limitations.

2 Model development

The development of the DWES has taken part within the Max Planck Institute – Hydrology Model (MPI-HM). The MPI-HM is a global hydrological model which solves the land surface water balance for 0.5° grid cells and a daily time step. It does not consider any energy balance calculations. The model consists of a simplified land surface scheme (Hagemann and Dümenil Gates, 2003) which calculates vertical water fluxes like evapotranspiration (ET) or runoff and the Hydrological Discharge Model (HD-Model) (Hagemann and Dümenil, 1998) which is a state of the art river routing model. The HD-Model is responsible for the lateral water transport from upstream to downstream grid cells. Both parts are coupled via the DWES and share a joint wetland water storage. In our study, the MPI-HM is not coupled to a global climate model. Thus, it requires daily fields of surface temperature, precipitation and potential evapotranspiration (PET) as forcing data. While temperature and precipitation have been taken directly from the Watch Forcing Dataset (Weedon et al., 2011), PET had to be calculated from other variables of this dataset using the Penman-Monteith equation. All simulation were conducted for the period from 1958 to 1999.

Currently, the DWES considers only those wetlands which are inundated for at least some time during the year. Wetlands without surface water are not accounted for. Additionally, the scheme does not distinguish between different types of surface water bodies.

HESSD
9, 405–440, 2012

2.1 Wetland dynamics

The DWES combines a physical and a statistical approach to account for wetland dynamics. The physical approach is based on the wetland water balance as shown in Fig. 1. Here, the change in the wetland water storage ΔS in the time period Δt is given as

$$\Delta S = (P - \mathrm{ET} - D + I_{\mathrm{lat}} - O_{\mathrm{lat}}) \times \Delta t \quad (1)$$

where P is precipitation, D is sub-surface drainage and I_{lat} and O_{lat} are the lateral inflow and outflow of water, respectively. The MPI-HM separates precipitation into rainfall and snowfall depending on temperature. As the MPI-HM is not able to simulate the freezing of wetlands, snowfall would add directly to the wetland water storage and lead to a too high inflow during winter. This behaviour is corrected by allowing for a virtual snow layer on top of the wetland. This layer is based on the degree day approach. Snowfall is stored there and only liquid precipitation and snow melt contribute to the wetland storage. ET and drainage depend on the water saturation of the wetland. When the wetland water table is below the soil surface both water fluxes are scaled according to the actual soil moisture content and reach their maximum values as soon as surface water exists. For ET the maximum is given by the Penman-Monteith evaporation following the methodology of Weedon et al. (2011). For drainage the scheme after Dümenil and Todini (1992) is used. As the soils below wetlands usually have a low permeability (Ingram, 1978), the maximum drainage is reduced to 10 % of the maximum drainage of non wetland areas. These fluxes are one-dimensional and from now on called vertical fluxes. When converting them into volume fluxes they are multiplied with the wetland area. Thus, they depend linearly on the extent of the wetlands.

The lateral flows are computed by the MPI-HM as volume fluxes. The overall amount of lateral inflow into a grid cell is determined by the outflows of its upstream grid cells. Within the grid cell it has to be divided between the wetland storage and the river flow storage. Several approaches were tested to find a valid scheme for this partition. In

HESSD
9, 405–440, 2012

the final concept, the lateral wetland inflow is determined as

$$I_{lat} = I_{gb} \times f_{wetl}^{z} \quad (2)$$

where I_{gb} is the overall inflow into the grid cell, f_{wetl} is the wetland covered grid cell fraction and z is the inflow exponent. The lateral outflow is only computed for wetlands with surface water in the storage S and calculated as

$$O_{lat} = \frac{S}{k} \quad (3)$$

$$k = \frac{\Delta x}{v} \quad (4)$$

$$v = c \times h^{\frac{2}{3}} \times s^{\frac{1}{2}} \quad (5)$$

where k is the retention time of the wetland which depends on the distance Δx between the grid cells and the water flow velocity v. The velocity v is computed similar to the Manning-Strickler equation (e.g. Gioia and Bombardelli, 2001) with c as the flow coefficient, h as the wetland water level and s as its mean slope. Using these equations the lateral water flows depend in a non-linear relation on the surface area as well as on other variables.

The different area dependencies of vertical and lateral flows result in the existence of a stable wetland surface area for which the inflows and outflows are in equilibrium (see Fig. 2). Wetlands which are smaller than this size would have a net water volume increase and grow until they reach the equilibrium extent and vice versa for larger wetlands. The size of the equilibrium extent is not constant but varies with the climatic conditions in the grid cell. When these are changing the wetland adapts by changing its surface area. Its reaction depends on the relation between its surface area and water volume and is given explicitly by the geometry of the wetland. However, the horizontal resolution of global climate and hydrology models is too coarse to represent the topography in sufficient detail. For this reason, we need an alternative measure about how fast the wetland area may adapt to changes in its water balance.

HESSD
9, 405–440, 2012

We assume that wetlands on plains react faster to changes in surface water volume compared to wetlands in mountainous regions. In the first case, additional water is distributed over a large plain without major water level differences. Thus, almost all water is used to increase the wetland area. In the second case, the wetland is confined by higher slopes. Here, part of the new water volume is needed to raise the water table. Now, only the residual water extents the surface area and the resulting extent growth is diminished. The behaviour can be parametrized using the sub-grid distribution of slope within every model grid cell. We derived those sub-grid slope data from the GTOPO30 topography (Gesch et al., 1999) which provides 3600 slope values per 0.5° grid cell. In order to decrease the computational costs, the slope distribution is not used directly but it is approximated with a shape function (see Fig. 3). The function describes the actual sub-grid slope s for a given grid cell fraction f as

$$s(f) = \max\left[\left(1-(1-f)^{\frac{1}{b}}\right)\cdot s_{\text{range}} + s_{\text{min}}, 0.\right], \text{ with} \quad (6)$$

$$s_{\text{range}} = s_{\text{max}} - s_{\text{min}} \quad (7)$$

where b is a shape parameter, s_{range} is the difference between maximum slope s_{max} and minimum slope s_{min} of the grid cell. For the majority of grid cells this function can be fitted very well to the sub-grid slope distribution with an asymptotic standard error below 1 %.

Then, we relate the relative change of wetland surface area $\Delta A/A$ to the relative change in wetland water volume $\Delta V/V$

$$\frac{\Delta A}{A} = \frac{\Delta V}{V} \times C, \text{ with} \quad (8)$$

$$C = \frac{1}{1 + s(f_{\text{w}}) \times S_{\text{sl}}} \quad (9)$$

where C is a scaling factor which accounts for the influence of slope on the surface area response of the wetlands with s being the maximum slope of the wetland covered

HESSD
9, 405–440, 2012

grid cell fraction f_w and S_{sl} being the slope sensitivity which is depending on the model resolution. Figure 4 demonstrates the effect of the sub-grid slope approach for a grid cell test case. In the first part of the time series moist climate conditions prevail. Thus, the water balance is mostly positive resulting in a growing wetland. The wetland extent change reacts strongly to wetland volume change in the beginning but the reaction becomes weaker when the wetland spreads onto the steeper parts of the grid cell. In the second period of the test case the climate is set to drier conditions resulting in a negative water balance and in shrinking wetlands. During its retreat to the flat plains of the grid cell the response of area change to volume change becomes stronger again.

2.2 Model optimization

The DWES is designed to work on the large scale rather than on process scale. Thus, it does not explicitly resolve the hydrological processes in wetlands but has to parametrize them. Amongst others, these parametrizations have to account for the actual model resolution. The parameter optimization was applied for the exponent z of the inflow scheme (Eq. 2), the flow coefficient c of the lateral wetland outflow (Eq. 5) and the slope sensitivity of the sub-grid slope approach (Eq. 9). All three parameters influence the simulated wetland extent. Although it would be possible to calibrate these parameters on grid cell scale against wetland observations, we decided against this method due to the large uncertainty in those observations (Lehner and Döll, 2004; Frey and Smith, 2007). Instead, we utilized river discharge measurements and derived globally constant values for them. While global values can not account for the vast diversity of wetland types, they are much more robust against outliers caused by errors in the observations or by processes which are not taken into account by the model. Furthermore, time series of river discharge are not available on grid cell scale, but only as integrals over catchments.

The optimization took place in two steps. First, the inflow exponent and the flow coefficient were considered using a static version of the wetland extent scheme (SWES) with prescribed wetland fractions. A simulation series was conducted in which both

HESSD
9, 405–440, 2012

parameters were varied systematically. The simulated river discharge of all simulations was compared to observations from the Global Runoff Data Centre (2011). However, deviations of simulated from observed river discharge are not caused solely by the wetland parameters but also by other missing processes in the model or biases in the forcing data. Furthermore, the observations themselves might have a considerable uncertainty (Di Baldassarre and Montanari, 2009). Consequently, only the peak flow and the amplitude of the river discharge seasonality were taken into account which are known to be sensitive to wetland influence (Bullock and Acreman, 2003). Both were combined in a cost function γ that evaluates the agreement between the observation O and the simulation S with a given pair of parameter values z and c for a river catchment R as:

$$\gamma(z,c,R) = \left(\frac{|P_S - P_O|}{6} + 1\right) \times \left(\frac{|\mathrm{VAR}_S - \mathrm{VAR}_O|}{\mathrm{VAR}_S + \mathrm{VAR}_O} + 1\right) \quad (10)$$

with P as the peak month of the river discharge curves and VAR as their monthly variances. The result of $\gamma(z,c,R)$ becomes smaller with less differences between simulation and observation. For every simulation, $\gamma(z,c,R)$ was weighted by the wetland fraction for the respective catchment and, finally, averaged over all river basins. This analysis considered only those river catchments which include at least 40 grid cells and have a similar area (±10 %) in model and observations. It has to be taken into account that global wetland observations are still quite uncertain (Frey and Smith, 2007) and differ significantly from each other (Lehner and Döll, 2004). Thus, the analysis was done using 4 different wetland observations as boundary data for the SWES. These data sets are listed at the beginning of Sect. 2. When comparing the cost values for the different maps, the best agreement on a low cost value was found for $z = 2$ and $c = 1.1\,\mathrm{m}^{1/3}\,\mathrm{s}^{-1}$.

In a second step, the slope sensitivity S_{sl} was optimized using the DWES. During this analysis, the river discharge simulation was not compared to observations anymore, but directly to the range of discharge curves which were generated by the optimized SWES. As all these curves were produced by the same model and forcing

HESSD
9, 405–440, 2012

data, the discharge curves can be evaluated using the normalized root mean square error instead of the cost function. The smallest error was achieved for simulations with $S_{sl} = 1$.

3 Model validation

In order to validate the DWES, its results are compared to global observations of wetland extent and their seasonality. The analyses focuses mostly on large scale structures but also some water bodies at grid cell scale are taken into account. For the validation simulations, the same forcing data and time period were used as for the optimization procedure.

3.1 Global wetland distribution

Starting with the global scale analysis, we compare the simulated wetland fraction with four datasets of global wetland and inundation observations. While these data sets have already been used as boundary conditions in the optimization procedure, the DWES is not calibrated to match them. Thus, they can still be applied as independent basis for the validation.

Table 1 gives an overview about the simulated and observed wetland cover for every continent. The largest wetland fraction is simulated for North and South America. For North America, Europa and Australia the difference between simulated and observed wetland fraction range within the standard deviation of the observations. The model strongly overestimates wetland extent in South America and Africa but finds a too small wetland extent in Asia. On global scale the mean model results are close to the observations. Generally, a high standard deviation is found for the wetland observations (between 20 % to 50 % of the ensemble mean value) indicating a considerable uncertainty between the observational data sets.

HESSD
9, 405–440, 2012

When analyzing the large scale pattern of wetland distribution, all observation data show most wetlands in the northern high latitudes. They are located especially in Northern America and Northern Europe as well as in Western and Eastern Siberia. Furthermore, wetlands occur in the tropical regions of South America and Africa but here the datasets differ strongly in the absolute extent of those wetlands. Some of the datasets also indicate extensive wetlands in Southeastern Asia. Figure 5 displays the observed and simulated wetland fractions. The model computes increased wetland fractions mostly for the same regions which are wetland focus regions in the observations. The best agreement is visible for North America where not only the pattern of wetland distribution is matched but also its mean extent. The wetland clusters in the north of the Eurasian continent are well represented but with a slightly lesser extent than observed. Likewise, too few wetlands are simulated for Southeastern Asia especially in China and the region between Vietnam and Myanmar. On the southern hemisphere the simulated wetlands concentrate in the Amazon and Congo catchments. While this location is confirmed by most observations, the overall extent is strongly overestimated by the model. These simulation results demonstrate that the DWES is able to reproduce the large scale wetland patterns.

An analysis of the zonal mean wetland fraction (see Fig. 6, top) again illustrates the differences between the four observational data sets with deviations up to 10 % of the grid cell area. On the northern hemisphere the simulated wetland fractions mostly lie within the range of observations but usually below their ensemble mean. Alike to the observations, the largest wetland fractions are computed between 40° and 70° N. However, between 10° N and 20° S the DWES overestimates the wetland extent by a factor of three compared to the ensemble mean.

We also investigate the spatial agreement between simulation and observation. Figure 6 (bottom) shows the linear correlation coefficients of the wetland fraction along the latitudes for the different wetland datasets. Considering only the correlation between the observations, significant differences already indicate deviations in the observed locations of the wetlands. At some latitudes, e.g. between 40° and 50° N almost no

HESSD
9, 405–440, 2012

correlation is seen whereas at other latitudes most observational data sets are highly correlated. The figure also shows that the correlation coefficients between simulation and observations lie in the same range as those between observations. Focusing on the correlation between the simulation and the ensemble mean of the observations, the highest correlation coefficient of about 0.5 is found for the high northern latitudes while the lowest correlations concentrate directly south of the equator.

3.2 Seasonal variations in wetland extent

Beside the simulation of wetland extent, the wetland seasonality is another key aspect of the DWES. Here, the model validation is restricted to one dataset, the SIND, because it is currently the only global dataset with monthly values of inundated area. Figure 7 displays the climatologies of simulated and observed wetland extent. While the simulated wetland extent has two peaks at early summer and during autumn on the northern hemisphere, the observations show only one maximum at the end of summer. However, the satellites are not able to identify wetlands below snow cover. Thus, snow covered grid cells have been masked out in the observational data (Papa et al., 2010). After applying the same snow mask for the simulated wetland fractions, both datasets agree well in both the magnitude and timing of the wetland extent variations although the simulation shows a higher overall extent. For the southern hemisphere the snow mask has no significant effect on the simulation results. Here, the wetland extent and its variation magnitude are strongly overestimated by the model but the timing of maximum and minimum wetland fractions coincide with the SIND data.

We enhance the analysis by calculating the spatial distribution of the temporal correlation between simulation and observation (not shown). In order to increase the robustness of the analysis, the mean wetland extent is calculated for every grid cell and month as an average over the grid cell itself and its 8 neighbour grid cells. Thus, spatial offsets of just one grid cell are neglected. Additionally, the snow mask is applied. For most of the large scale wetland clusters a good temporal correlation is achieved, but in between those areas pronounced regions of insignificant correlations are found.

HESSD
9, 405–440, 2012

Examples for these regions are wide parts of Europe as well as some areas in South America, Africa and Australia. Additionally, insignificant correlations prevail north of 60° N. Investigating the reasons for this pattern, we find a strong impact of the snow mask. As its application decreases the number of months that can be used in the correlation analysis, the correlation becomes less significant. Occasionally, the significance is biased towards higher values for larger wetlands. However, the latter feature is not a robust result. Neglecting all insignificant correlations, a global mean correlation coefficient of 0.70 is computed.

The seasonal variations in wetland extent are displayed in Fig. 8. Here, two large scale processes are represented by the simulation. In the northern high latitudes wetland fractions decrease during DJF and subsequently increase during MAM starting from the south reaching the far north in JJA. This behaviour reflects the decreased wetland inflow during the cold season and the increased inflow during snowmelt. In the tropics the wetland extent follows the rainy and dry seasons which are caused by the movement of the Intertropical Convergence Zone. Here, the simulation shows decreased wetland fractions north of the equator in DJF and increased wetland fractions south of it. This pattern is mirrored during JJA.

3.3 Local scale simulations

In order to explore the limitations of our approach, we also investigate the model performance on the grid cell scale. Here, we validate the model against satellite based lake level variation data because these data are better available than long term time series of wetland water level observations. The observations were derived from different satellites by the GRLM (2011).

Figure 9 (top) displays the linear correlation coefficient between the observed and simulated monthly climatologies of water level variations for 79 lakes. For 12 lakes no surface water occurs in the model and about one third of all lakes do not show any significant correlation above the 90 % confidence level. More than half of the remaining lakes correlate very well with the simulation with coefficients above 0.8. The correlation

HESSD
9, 405–440, 2012

of the remaining lakes is at least 0.5 with the exception of three lakes which show a significant negative correlation. Investigating the reasons for the insignificant correlations, we find that insignificant results occur preferably for lakes with a mean simulated water throughflow below 300 $m^3 s^{-1}$. As the water throughflow is connected to the size of the respective upstream catchment, a similar effect is seen there, too. Insignificant correlations are mostly found for catchments smaller than 0.2×10^6 km^2 while significant results dominate for larger upstream catchments.

While the timing of intra-annual water level dynamics is simulated well for about one third of the lakes, the DWES underestimates the range of these variation for almost every location. Analyzing this model behaviour, we find good agreements only for those lakes which have a low variability in the observations or are simulated with a large grid cell fraction. Here, the water throughflow does not play any significant role.

Additionally, the wetland fraction is compared to the observed lake fraction in the GLWD on grid cell scale (see Fig. 9, bottom). Focusing on locations where lakes are present in the observation and simulation, about one third of the lakes agree well in grid cell fraction with a deviation less than ±12.5 %. Another third show deviations that are less than ±50 %. Despite of these absolute differences, a significant correlation coefficient of 0.78 is obtained. Similar to the significance of lake level variations, we find the smallest wetland fraction deviations for wetlands with a high water turnover larger than 300 $m^3 s^{-1}$. However, no strong relation to the simulated wetland fraction is visible. Although larger wetlands are usually simulated with a smaller difference to the observations, the water turnover rate seems to be the dominant factor that determines the simulation quality on local scale.

3.4 Wetland impact on river discharge

As river discharge has already been used for the model parameter optimization, it has only limited applicability for the validation. However, its analysis allows to investigate the influence of wetlands on the simulated river discharge and to give a first estimate of the performance of the model.

HESSD
9, 405–440, 2012

Focusing on a selection of about 100 major river catchments, we find that almost all of them are sensitive to wetland influence. Generally, the mean river discharge decreases in the presence of wetlands. Most catchments only experience a small decrease up to 5 % of the annual discharge but also large changes up to 25 % decrease occur. Similar effects are also apparent in the discharge seasonality. Comparing the variance of river discharge, the majority of catchments reveals a decrease between 0 % and 45 % with a maximum decrease of 90 %. Additionally, the peak flow is simulated at later time steps when the DWES was active. For most catchments this delay is less than one month.

A minority of the catchments shows the opposite reaction in the presence of wetlands. Here, increased mean flow and seasonality are evident but no earlier peak flows can be recognized. The strongest increases are up to 20 % for the mean flow and up to 40 % for the seasonal variations. Examples for this behaviour are the catchments of the Blue Nile, the Sao Francisco and the Colorado River.

As the river discharge has been used to optimize the DWES's parameters, an improvement of its simulation is expected. Again, we applied the cost function (see Eq. 10) to compare the climatologies of simulated river discharge with the observed river discharge (Global Runoff Data Centre, 2011). For most catchments, the change in simulation error ranges within −8 % and 2 % with extremes up to −45 % and 61 %. We do not find any significant correlation of model improvement with the catchment's simulated wetland fraction or area. However, the strongest influence of the DWES is found for rivers with a large catchment area. Here, the discharge simulation of rivers like Amazon and Ob is closer to observations in terms of peak flow and seasonality. Other large catchments, e.g. Mackenzie and Mississippi are simulated with less agreement. On average, there is a small improvement of the discharge simulation which is almost balanced by those catchments with degraded results.

HESSD
9, 405–440, 2012

4 Discussion

In terms of large scale features, the DWES reproduces the wetland distribution successfully. However, regional deficits in simulation performance have been revealed during the validation which need to be discussed. Another important question is whether the simulation of wetlands might cause hydrological feedbacks in the climate system, e.g. due to enhanced evapotranspiration. As our study is conducted using a global hydrological model with prescribed climatic forcing, we cannot directly calculate any large scale hydrological feedbacks of wetlands. Still, we aim to identify possible connections between the wetlands and the remaining earth system.

4.1 Feedbacks to other earth system components

There are a number of possibilities how wetlands might feedback to the climate system. Several studies focus on changes in atmospheric methane concentration (e.g. Gedney et al., 2004; Finkelstein and Cowling, 2011) and the effect on mean surface temperature as a result of the change in radiative forcing. Coe and Bonan (1997) simulated the influence of surface water on Mid-Holocene climate conditions and found an increase in net surface radiation, latent heat and humidity as well as an decrease in the sensible heat flux. These changes lead to a cooling of the atmosphere and an alteration of the atmospheric flows resulting in changes in the regional precipitation patterns. Dadson et al. (2010) and Taylor (2010) concentrated on the Niger inland delta. The authors connected the seasonal inundation in this region with enhanced evaporation and an increase in cloud cover and convection. In our study we concentrate on hydrological feedbacks between wetlands, the atmosphere and the ocean. Here, we compare the results of the dynamical wetland simulation to a control simulation without wetlands.

In our model, the only feedback path from wetlands to the atmosphere is via the ET. We find that the simulation of wetlands increases the annual ET by 4.5 mm on average over the global land surface without Antarctica. The largest ET increase occurs during the summer months. For most of the land surface, this ET anomaly is below

HESSD
9, 405–440, 2012

0.1 mmd^{-1}. However, regionally much stronger effects occur, for instance, in high latitudes of North America and Eastern Siberia. Due to open water in the simulated wetlands, they almost evaporate at the potential rate resulting in ET anomalies exceeding 1.0 mmd^{-1} during the summer months. In contrast, small negative ET anomalies are simulated during dry spells for some grid cells in equatorial regions. Here, open water surfaces vanish during the summer reducing ET and soil moisture significantly. While the soil moisture is similarly low in both simulations, the larger vegetation skin reservoir of the land surface in the control run evaporates water more easily than the wetland soils of the DWES simulation. However, this effect occurs only sporadically and does not effect the overall ET increase significantly. In summary, we expect the additional ET provided by the wetlands to locally increase the air humidity and cloud cover. This results in lower surface temperatures due to evaporative cooling and less radiation reaching the surface. Thus, less energy is available for evaporation and more water is stored within the wetlands instead of being transported into the atmosphere. Eventually, this results in a wetter and cooler state of the surface and therefore in a stabilization of local climate conditions.

As more water is evaporating, the runoff from the land surface is decreased. The surface runoff shows negative anomalies with mean values up to −2 mmd^{-1}. The mean drainage declines by up to −0.5 mmd^{-1} because wetland soils are parametrized with a lower hydraulic conductivity. In spite of this, a positive drainage anomaly is found in some wetland regions. Here, wetlands are sustained by river flows. In the standard MPI-HM version, water that once entered the river routing scheme is not available to the land surface anymore but flows via the river network into the ocean. However, in the DWES river flow can recharge wetlands and thus increase ET and drainage in downstream grid cells. Thus, an increase in drainage is not so much a result of the wetland simulation but rather enabled by the coupling between the lateral and vertical water flows. Although positive drainage anomalies are just around 0.2 mmd^{-1}, they partly contribute to an increase of river flow in some catchments (see Sect. 3.4).

HESSD
9, 405–440, 2012

Due to the runoff decrease, the river discharge into the oceans declines, too. Here, about 530 $km^3 a^{-1}$ less water reach the oceans. This decrease balances most of the ET increase of 670.9 $km^3 a^{-1}$. Again, some grid cells are found which show the opposite behaviour. They are located in regions where either wetlands are simulated with a large extent and a considerable water turnover or steep slope conditions prevail that facilitate fast water transport. In these catchments, water is transported more efficiently in the wetlands than via overlandflow. Together with the positive drainage anomaly, the bypass of overland flow causes locally increased river discharge. This model feature is supported by a Bullock and Acreman (2003) who reported about observations displaying the same behaviour for some headwater wetlands. As the overall inflow decline is just about 1 % of the overall ocean inflow, we do not expect any significant influence on the ocean in terms of hydrology. However, the decline might have implications for the nutrient or sediment transport into the ocean.

4.2 Limitations of the DWES

The simulation results show a pronounced underestimation of the wetland extent in Southeastern Asia. Here, extensive wetlands exist but these are mostly artificially formed (Mudge and Adger, 1995). They are not captured by the model because the MPI-HM simulations do not account for human impacts. The extent overestimation in the Eastern USA and Western Europe can be attributed to the same shortcoming. In these regions, existing wetlands were artificially drained (Finlayson and Davidson, 1999). Some regions lost more than 50 % of their wetland area, e.g. in the Southwestern USA (Dahl and Allord, 1996). However, these wetland losses were mainly caused by human impact rather than by climate change. Thus, the DWES represents potential wetlands which could be sustained by climate conditions but were removed by landscape management.

Another major deficit is evident for the tropical regions where the model overestimates the observed wetland fraction by a factor of three. Here, too much surface water is available in the model indicating either a wet bias in the precipitation forcing or a

HESSD
9, 405–440, 2012

too low PET. The PET is calculated offline using the Penman-Monteith evaporation. Following Weedon et al. (2011), we use globally constant parameters of short grass for the vegetation height and the surface resistance. However, the major land cover type in these areas is tropical forest. As Amazonian rainforest usually has a significantly higher ET than grassland (e.g. Costa and Foley, 1997; von Randow et al., 2004), PET is probably underestimated by the model leading to too extensive wetlands. A third error source could have been an underestimated river flow out of the basin. However, the simulated river flow for the Amazon and Congo catchments exceeds the observed values and, thus, this possibility can be ruled out.

Except for the tropics, the simulated zonal mean wetland fraction is usually close to the lower limit of the observational range. This is especially pronounced in the high northern latitudes indicating that the DWES either lacks surface water or does not capture all types of wetlands. The second possibility seems more reasonable as the northern regions are dominated by water logged peatlands rather than wetlands with explicit surface water. Indeed, the model is limited to the simulation of the latter type because its bucket like soil scheme does not include subsurface wetland dynamics. Conclusively, the DWES neglects most peatlands causing a general underestimation of wetland extent in the respective areas.

The simulation results demonstrate the model's ability to simulate even some small wetlands and lakes under certain conditions. Beside a large water turnover which is needed for a robust wetland simulation, the model only works successfully for lakes which are in equilibrium with actual climate conditions. Among the 12 lake locations where the DWES does not simulate any surface water, some lakes could not be identified because they are not supported by the climate conditions during the simulation period. Examples for these are the Lake Aral and the Lake Chad. As these lakes rely on their water storage of former times, a model cannot simulate their extent using today's climate as forcing without realistic surface water initialization. Other lakes are artificial reservoirs and were not considered during the development of the DWES.

HESSD
9, 405–440, 2012

A further limitation is that the model captures only the seasonality of lake levels but underestimates their range. As this deficiency is less for larger simulated wetland fractions, we assume it might be related to the sub-grid distribution of water bodies. In our sub-grid slope approach we neglect the information about the exact positioning of wetlands within the grid cell and, thus, we cannot know whether all surface water is concentrated in a single wetland or distributed into several water bodies. Instead, the variation of water level is computed as average for all surface water bodies in the whole grid cell. In contrast, the satellite observations consist of average lake level variations over less than 0.3 km^2 (GRLM, 2011), which is much smaller than the average 0.5° grid cells. Thus, they probe only a single lake whose water level variations are not necessarily connected to the average variations in the grid cell area, which may lead to very different results. This deviation becomes smaller with larger lakes because then simulation and observations relate to the same area.

The river discharge analysis revealed no distinct improvement of its simulation. We found that the impact of wetlands changes the river flow only in catchments with a mean simulated wetland area greater than 1000 km^2. However, the number of wetland influenced catchments whose river discharge simulation is improved is about equal to the number of worse simulated ones. On the one hand this is indicating that the restriction to global parameters does not account for the vast diversity of different wetland types. Thus it might be necessary to develop more specific parameters for different catchments in future model versions. On the other hand, we found no strong changes in artificially influenced river catchments like Nile, Amu Darya and Rhine, which all are either used for irrigation or are strongly regulated. Human influences are not captured by the MPI-HM and therefore river discharge in those catchments cannot be simulated correctly. Here, the application of global parameters prevents the DWES from counteracting simulation errors that are not connected to wetlands.

HESSD
9, 405–440, 2012

5 Conclusions

The scope of this study was the development and validation of a global hydrological scheme that accounts for dynamical processes in wetland hydrology. Based on the newly developed flux equilibrium and sub-grid slope approaches, the DWES is able to transfer changes in the wetland water balance into variations of its surface extent. Therefore, not only the water table but the whole wetland might now react dynamically to changes in the earth's climate.

We found that the simulated wetland distribution as well as their seasonal variations agree well with the range of observations. However, the wetland extent is overestimated in the tropics. Additionally, water level variations were investigated for single grid cells. Their simulated seasonality shows a high correlation to satellite observations but the overall range of water level fluctuations is underestimated. Limitation of the DWES are the restriction to wetlands with surface water and the neglection of human impacts. In further studies we will aim to extent the DWES into the soil and to include peatland dynamics. Additionally, the scheme will be implemented into the coupled climate model ECHAM6/JSBACH.

Acknowledgements. This research was undertaken as part of the European Union (FP6) funded Integrated Project called WATCH (contract number 036946). We thank Catherine Prigent for kindly providing the monthly inundation dataset to us and for her valuable comments about this paper.

The service charges for this open access publication
have been covered by the Max Planck Society.

References

Bohn, T., Lettenmaier, D., Sathulur, K., Bowling, L., Podest, E., and McDonald, K.: Methane emissions from western Siberian wetlands: heterogeneity and sensitivity to climate change, Environ. Res. Lett., 2, 045015, doi:10.1088/1748-9326/2/4/045015, 2007. 407, 408

HESSD
9, 405–440, 2012

Bonan, G.: Sensitivity of a GCM simulation to inclusion of inland water surfaces, J. Climate, 8, 2691–2704, 1995. 407

Bowling, L. and Lettenmaier, D. P.: Modeling the Effects of Lakes and Wetlands on the Water Balance of Arctic Environments, J. Hydrometeorol., 11, 276–295, doi:10.1175/2009JHM1084.1, 2010. 408

Bullock, A. and Acreman, M.: The role of wetlands in the hydrological cycle, Hydrol. Earth Syst. Sci., 7, 358–389, doi:10.5194/hess-7-358-2003, 2003. 407, 414, 423

Coe, M. and Bonan, G.: Feedbacks between climate and surface water in northern Africa during the middle Holocene, J. Geophys. Res. D Atmos., 102, 11087–11101, doi:10.1029/97JD00343, 1997. 407, 421

Costa, M. and Foley, J.: Water balance of the Amazon Basin: Dependence on vegetation cover and canopy conductance, J. Geophys. Res. D Atmos., 102, 23973–23989, 1997. 424

Dadson, S., Ashpole, I., Harris, P., Davies, H., Clark, D., Blyth, E., and Taylor, C.: Wetland inundation dynamics in a model of land surface climate: Evaluation in the Niger inland delta region, J. Geophys. Res. D Atmos., 115, D23114, doi:10.1029/2010JD014474, 2010. 421

Dahl, T. E. and Allord, G. J.: Technical aspects of wetlands. History of wetlands in the conterminous United States, National water summary on wetland resources, US Geological Survey Water-Supply Paper 2425, 1996. 423

Decharme, B., Douville, H., Prigent, C., Papa, F., and Aires, F.: A new river flooding scheme for global climate applications : Off-line evaluation over South America, J. Geophys. Res. D Atmos., 113, D11 110, doi:10.1029/2007JD009376, 2008. 407

Decharme, B., Alkama, R., Papa, F., Faroux, S., Douville, H., and Prigent, C.: Global off-line evaluation of the ISBA-TRIP flood model, Clim. Dyn., 1–24, doi:10.1007/s00382-011-1054-9, 2011. 408

Di Baldassarre, G. and Montanari, A.: Uncertainty in river discharge observations: a quantitative analysis, Hydrol. Earth Syst. Sci., 13, 913–921, doi:10.5194/hess-13-913-2009, 2009. 414

Dümenil, L. and Todini, E.: A rainfall-runoff scheme for use in the Hamburg climate model, in: Advances in theoretical hydrology – a tribute to James Dooge, edited by: Kane, J., Vol. 1 of European Geophysical Society Series of Hydrological Sciences, 129–157, Elsevier Science, Amsterdam, 1992. 410

Finkelstein, S. and Cowling, S.: Wetlands, temperature, and atmospheric CO2 and CH4 coupling over the past two millennia, Global Biogeochem. Cy., 25, GB1002,

HESSD
9, 405–440, 2012

doi:10.1029/2010GB003887, 2011. 421
Finlayson, C. M. and Davidson, N. C.: Global review of wetland resources and priorities for inventory: Summary report, in: Global Review of Wetland Resources and Priorities for Inventory, edited by: Finlayson, C. M. and Spiers, A. G., Vol. 177 of Supervising Scientist Report, 1–14, Canberra, 1999. 423
Frey, K. and Smith, L.: How well do we know northern land cover? Comparison of four global vegetation and wetland products with a new ground-truth database for West Siberia, Global Biogeochem. Cy., 21, GB1016, doi:10.1029/2006GB002706, 2007. 413, 414
Friborg, T., Soegaard, H., Christensen, T., Lloyd, C., and Panikov, N.: Siberian wetlands: Where a sink is a source, Geophys. Res. Lett., 30, CLM 5–1–CLM 5–4, doi:10.1029/2003GL017797, 2003. 407
Ringeval, B., Friedlingstein, P., Koven, C., Ciais, P., de Noblet-Ducoudré, N., Decharme, B., and Cadule, P.: Climate-CH4 feedback from wetlands and its interaction with the climate-CO_2 feedback, Biogeosciences, 8, 2137–2157, doi:10.5194/bg-8-2137-2011, 2011. 407
Gedney, N., Cox, P., and Huntingford, C.: Climate feedback from wetland methane emissions, Geophys. Res. Lett., 31, L20503, doi:10.1029/2004GL020919, 2004. 407, 421
Gesch, D., Verdin, K., and Greenlee, S.: New land surface digital elevation model covers the earth, Eos Trans. AGU, 80, 69–70, doi:10.1029/99EO00050, 1999. 412
Gioia, G. and Bombardelli, F. A.: Scaling and Similarity in Rough Channel Flows, Phys. Rev. Lett., 88, 14501–1–14501–4, doi:10.1103/PhysRevLett.88.014501, 2001. 411
Global Runoff Data Centre: Long-Term Mean Monthly Discharges and Annual Characteristics of GRDC Station, Tech. rep., Global Runoff Data Centre, Federal Institute of Hydrology (BfG), Koblenz, Germany, available at: http://www.bafg.de/cln_007/nn_298422/GRDC/EN/02__Services/02__DataProducts/LongTermMonthlyMeans/longtermmonthly__node.html?__nnn=true, 2011. 414, 420
Gorham, E.: Northern peatlands: role in the carbon cycle and probable responses to climatic warming, Ecol. Appl., 1, 182–195, doi:10.2307/1941811, 1991. 407
GRLM: USDA/FAS/OGA and NASA Global Agriculture Monitoring (GLAM) Project. Lake and reservoir surface height variations from the USDA's Global Reservoir and Lake (GRLM) web site. Altimetric lake level time-series variations from the Topex/Poseidon, Jason-1, Jason-2/OSTM, and Geosat Follow-On (GFO) missions., available at: http://www.pecad.fas.usda.gov/cropexplorer/global_reservoir/, 2011. 418, 425
Hagemann, S.: An improved land surface parameter dataset for global and regional climate

HESSD
9, 405–440, 2012

models, MPI-Report 336, Max Planck Institute for Meteorology, Hamburg, Germany, 2002. 408
Hagemann, S. and Dümenil, L.: A parametrization of the lateral waterflow for the global scale, Clim. Dynam., 14, 17–31, doi:10.1007/s003820050205, 1998. 409
Hagemann, S. and Dümenil Gates, L.: Improving a subgrid runoff parameterization scheme for climate models by the use of high resolution data derived from satellite observations, Clim. Dynam., 21, 349–359, doi:10.1007/s00382-003-0349-x, 2003. 409
Hagemann, S., Botzet, M., Dümenil, L., and Machenhauer, B.: Derivation of global GCM boundary conditions from 1 km land use satellite data, MPI-Report 289, Max Planck Institute for Meteorology, Hamburg, Germany, 1999. 408
Ingram, H.: Soil Layers in Mires – Function and Terminology, J. Soil Sci., 29, 224–227, doi:10.1111/j.1365-2389.1978.tb02053.x, 1978. 410
Kaplan, J.: Wetlands at the Last Glacial Maximum: Distribution and methane emissions, Geophys. Res. Lett., 29, 1079, doi:10.1029/2001GL013366, 2002. 407
Kleinen, T., Brovkin, V., and Getzieh, R. J.: A dynamic model of wetland extent and peat accumulation: results for the Holocene, Biogeosciences Discuss., 8, 4805–4839, doi:10.5194/bgd-8-4805-2011, 2011. 407
Lehner, B. and Döll, P.: Development and validation of a global database of lakes, reservoirs and wetlands, J. Hydrol., 296, 1–22, doi:10.1016/j.jhydrol.2004.03.028, 2004. 408, 413, 414
Levin, D., Hopper, I., Ernst, F., Trivett, M., and Worthy, N.: Evidence for a link between climate and northern wetland methane emissions, J. Geophys. Res. D Atmos., 105, 4031–4038, doi:10.1029/1999JD901100, 2000. 407
Matthews, E. and Fung, I.: Methane emission from natural wetlands: Global distribution, area, and environmental characteristics of sources, Global Biogeochem. Cy., 1, 61–86, doi:10.1029/GB001i001p00061, 1987. 408
Mishra, V., Cherkauer, K., and Bowling, L.: Parameterization of lakes and wetlands for energy and water balance studies in the great lakes region, J. Hydrometeorol., 11, 1057–1082, doi:10.1175/2010JHM1207.1, 2010. 407
Mudge, F. and Adger, W.: Methane fluxes from artificial wetlands: A global appraisal, Enviro. Manage., 19, 39–55, doi:10.1007/BF02472002, 1995. 423
O'Connor, F., Boucher, O., Gedney, N., Jones, C., Folberth, G., Coppell, R., Friedlingstein, P., Collins, W., Chappellaz, J., Ridley, J., and Johnson, C.: Possible role of wetlands, permafrost, and methane hydrates in the methane cycle under future climate change: A review, Rev.

HESSD
9, 405–440, 2012

Geophys., 48, RG4005, doi:10.1029/2010RG000326, 2010. 407
Papa, F., Prigent, C., Aires, F., Jimenez, C., Rossow, W., and Matthews, E.: Interannual variability of surface water extent at the global scale, 1993–2004, J. Geophys. Res. D Atmos., 115, D12111, doi:10.1029/2009JD012674, 2010. 417
Prigent, C., Matthews, E., Aires, F., and Rossow, W.: Remote sensing of global wetland dynamics with multiple satellite data sets, Geophys. Res. Lett., 28, 4631–4634, doi:10.1029/2001GL013263, 2001. 408
Prigent, C., Papa, F., Aires, F., Rossow, W., and Matthews, E.: Global inundation dynamics inferred from multiple satellite observations, 1993–2000, J. Geophys. Res. D Atmos., 112, D12107, doi:10.1029/2006JD007847, 2007. 408
Ringeval, B., De Noblet-Ducoudré, N., Ciais, P., Bousquet, P., Prigent, C., Papa, F., and Rossow, W.: An attempt to quantify the impact of changes in wetland extent on methane emissions on the seasonal and interannual time scales, Global Biogeochem. Cy., 24, GB2003, doi:10.1029/2008GB003354, 2010. 407
St-Hilaire, F., Wu, J., Roulet, N. T., Frolking, S., Lafleur, P. M., Humphreys, E. R., and Arora, V.: McGill wetland model: evaluation of a peatland carbon simulator developed for global assessments, Biogeosciences, 7, 3517–3530, doi:10.5194/bg-7-3517-2010, 2010. 407
Taylor, C. M.: Feedbacks on convection from an African wetland, Geophys. Res. Lett., 37, L05406, doi:10.1029/2009GL041652, 2010. 421
von Randow, C., Manzi, A., Kruijt, B., de Oliveira, P., Zanchi, F., Silva, R., Hodnett, M., Gash, J., Elbers, J., Waterloo, M., Cardoso, F., and Kabat, P.: Comparative measurements and seasonal variations in energy and carbon exchange over forest and pasture in South West Amazonia, Theor. Appl. Climatol., 78, 5–26, doi:10.1007/s00704-004-0041-z, 2004. 424
Weedon, G. P., Gomes, S., Viterbo, P., Shuttleworth, W. J., Blyth, E., Österle, H., Adam, J. C., Bellouin, N., Boucher, O., and Best, M.: Creation of the WATCH Forcing Data and its use to assess global and regional reference crop evaporation over land during the twentieth century, J. Hydrometeorol., 12, 823–848, 10.1175/2011JHM1369.1, 2011. 409, 410, 424
Yu, Z., Pollard, D., and Cheng, L.: On continental-scale hydrologic simulations with a coupled hydrologic model, J. Hydrol., 331, 110–124, doi:10.1016/j.jhydrol.2006.05.021, 2006. 408

HESSD
9, 405–440, 2012

Table 1. Mean simulated and observed wetland cover for different continents in percent of their land surface.

Continent	Simulation [%]	Obs. ensemble [%]
North America	9.74	9.06 ± 4.76
South America	15.91	5.39 ± 2.64
Europa	4.25	5.49 ± 1.26
Africa	4.79	2.87 ± 1.35
Asia	2.76	6.92 ± 2.13
Australia	1.56	1.94 ± 1.04
Global	6.17	5.78 ± 1.61

HESSD
9, 405–440, 2012

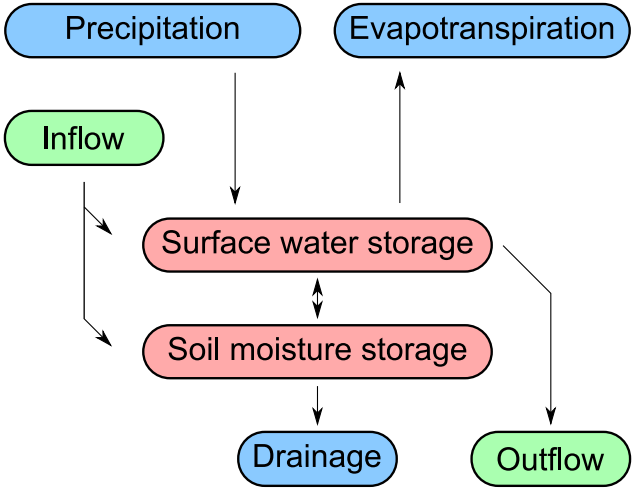

Fig. 1. Wetland water balance as simulated by the DWES. The green boxes indicate lateral water flows, the blue ones indicate vertical water flows, and the red ones indicate water storages.

HESSD
9, 405–440, 2012

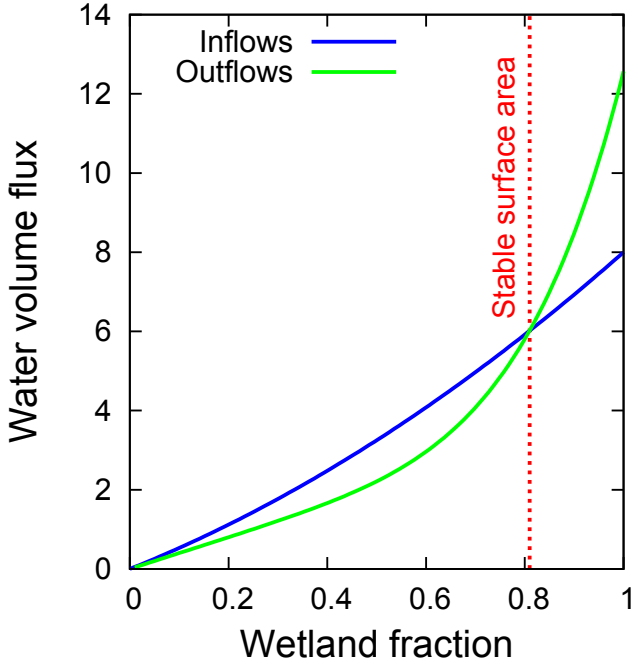

Fig. 2. Wetland water inflow (blue curve) and outflow (green curve) in dependence on its surface area for an example grid cell. The size of the equilibrium surface area (red line) depends on climatic conditions and the topography of the grid cell.

HESSD
9, 405–440, 2012

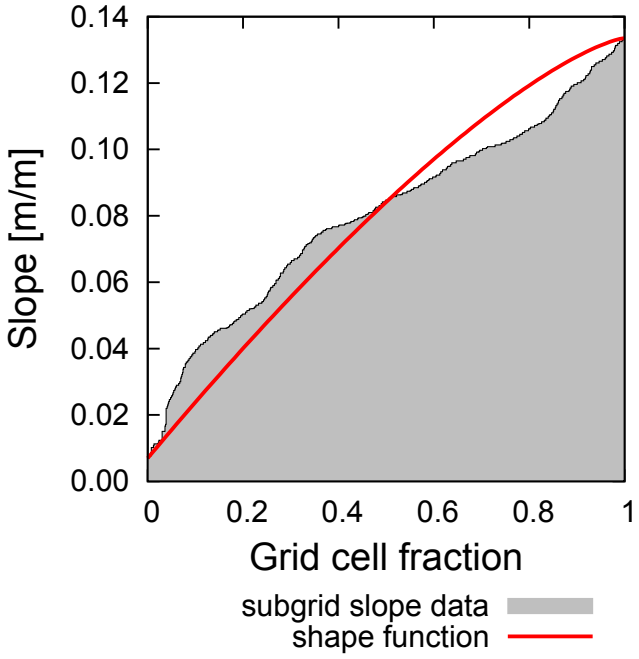

Fig. 3. Sub-grid slope distribution (gray) and shape function (red) for an example 0.5° model grid cell.

HESSD
9, 405–440, 2012

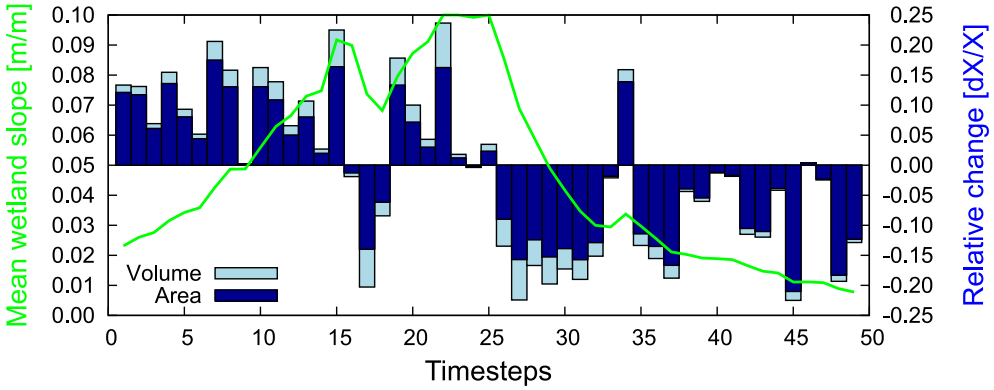

Fig. 4. Wetland dynamics for a one grid cell test case. The bars (light-blue) display the relative volume change within the wetland as derived by the water balance calculation. The dark-blue color indicate the relative area change as fraction of the relative volume change. The relative area change responds stronger to volume change when the wetland covered slope (green line) is low and weaker when the wetland covered slope increases.

HESSD
9, 405–440, 2012

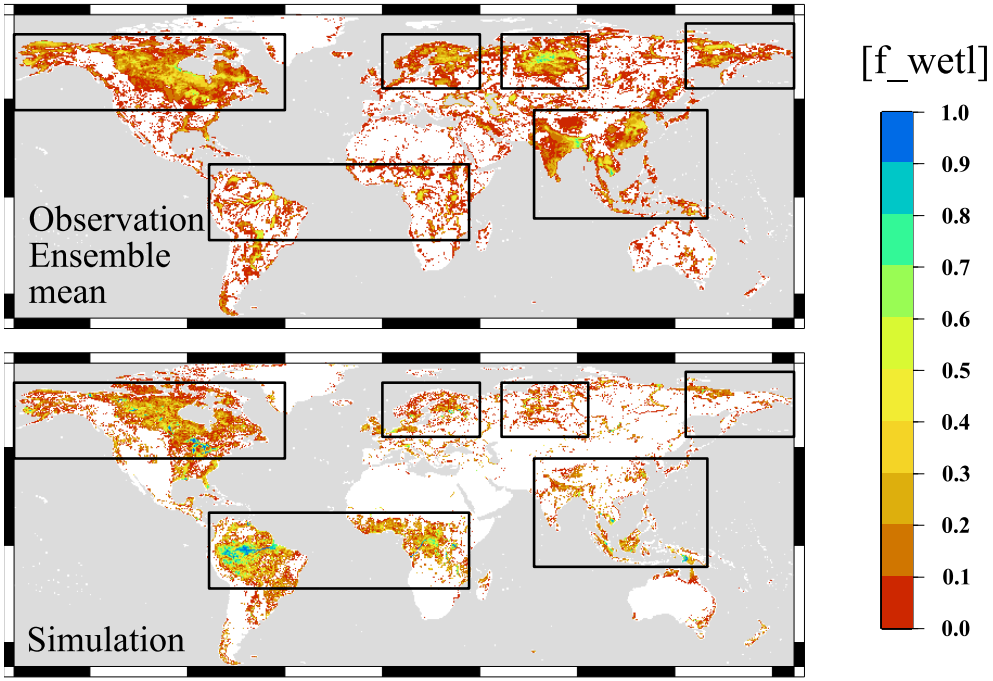

Fig. 5. Ensemble mean of observed wetland extent (top) and the simulated mean wetland extent (bottom). The colors indicate the wetland fraction for every 0.5°grid cell. The black boxes highlight regions of pronounced wetland occurrence.

HESSD
9, 405–440, 2012

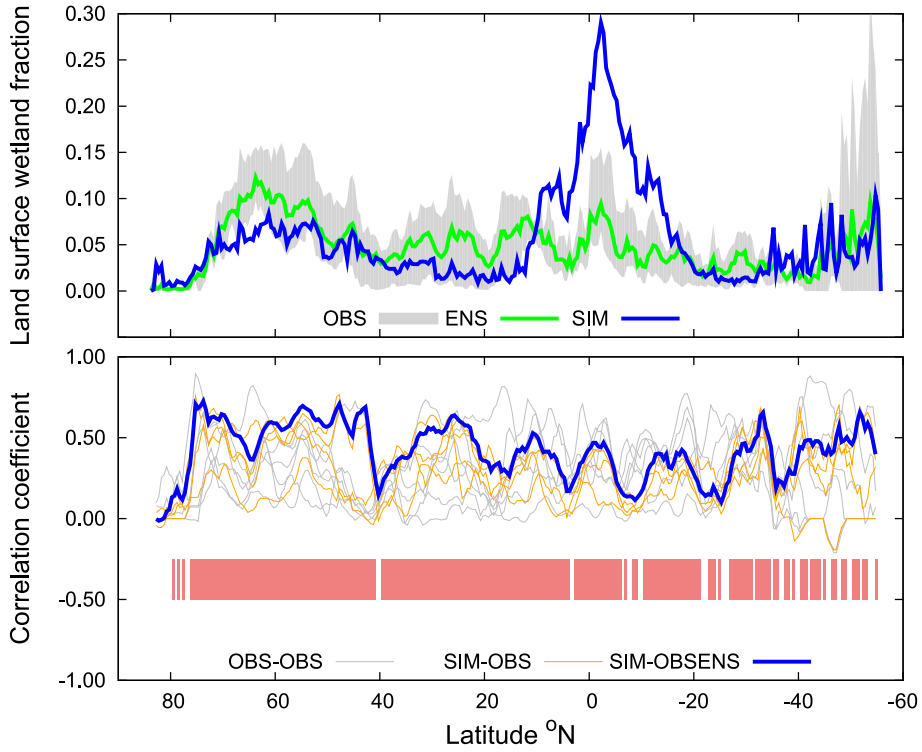

Fig. 6. Top: zonal means of wetland fraction for the simulation (blue), the ensemble mean of observations (green) and the range of the four observational data sets (gray). Bottom: zonal correlation between the simulated wetland extent and the ensemble mean of observations (blue), between the simulated extent and the four observation datasets (orange) and between the observations themselves (gray). Displayed are running means over 2.5 latitudes. The red boxes indicate latitudes where the correlation significance level between the simulation and the ensemble mean of observations is above 95 %.

HESSD
9, 405–440, 2012

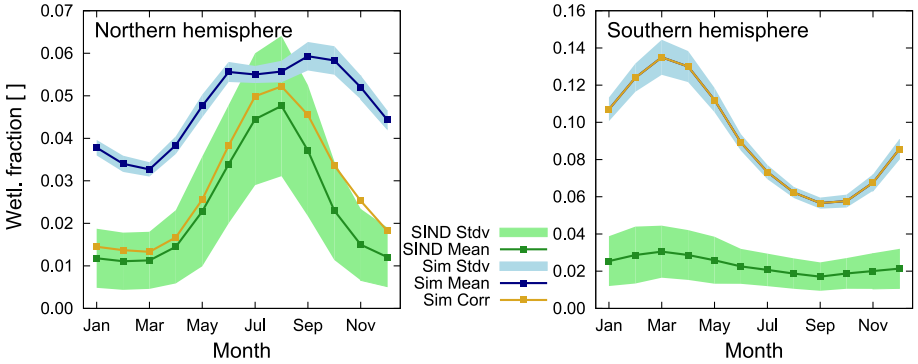

Fig. 7. Seasonality of wetland extent for the northern and southern hemispheres. The green color indicates the observations, the blue the simulations and the yellow line represents the simulations corrected with the snow mask, respectively.

HESSD
9, 405–440, 2012

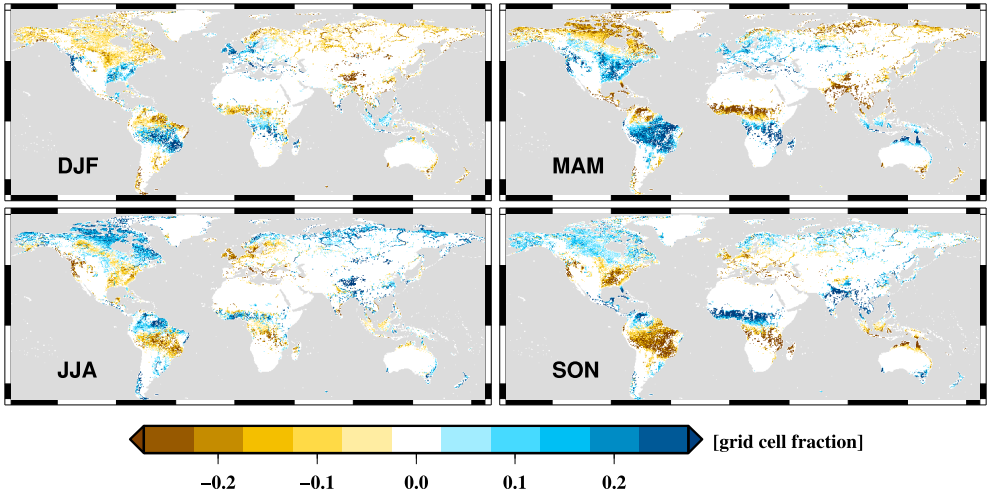

Fig. 8. Simulated deviation of the wetland fractions from its yearly mean for all seasons.

HESSD
9, 405–440, 2012

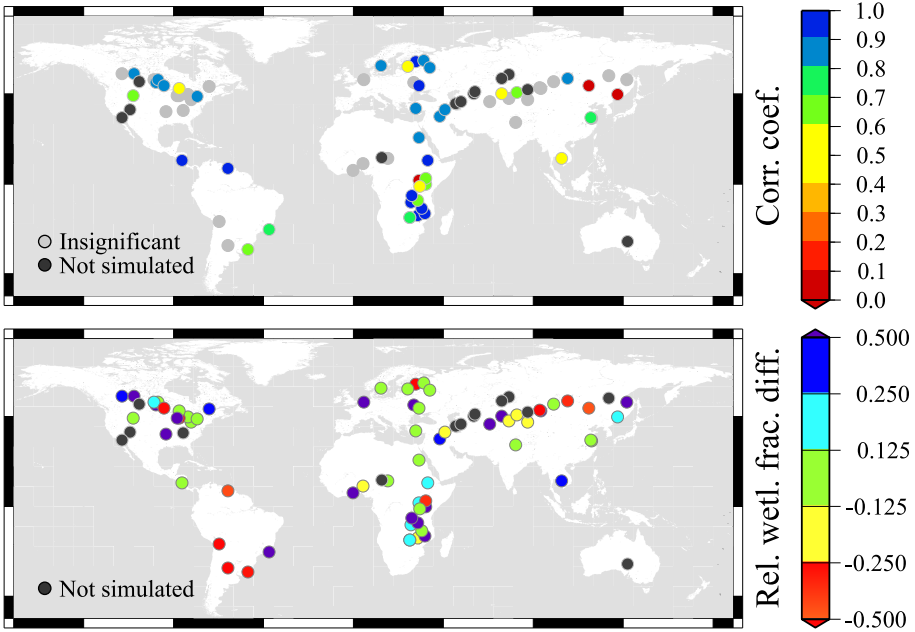

Fig. 9. Top: Map of investigated lakes. The color indicates the correlation coefficient between the simulated and observed lake level climatologies. Light gray points depict insignificant correlations. Dark gray points depict locations where no lake was simulated. Bottom: Relative difference between simulated and observed lake fractions (GLWD) for the same lakes as in the upper map.

HESSD
9, 405–440, 2012